Geophysical Research Letters

RESEARCH LETTER
10.1029/2024GL110453

Double Reflections in Polarized Radar Data Reveal Ice Fabric in the North East Greenland Ice Stream

Niels F. Nymand[1], David A. Lilien[2,3], Tamara A. Gerber[1], Christine S. Hvidberg[1], Daniel Steinhage[4], Prasad Gogineni[5], Drew Taylor[5], and Dorthe Dahl-Jensen[1,2]

[1]Niels Bohr Institute, University of Copenhagen, Copenhagen, Denmark, [2]Centre for Earth Observation Science, University of Manitoba, Winnipeg, MB, Canada, [3]Department of Earth and Atmospheric Sciences, Indiana University, Bloomington, IN, USA, [4]Alfred Wegener Institute, Helmholtz Centre for Polar and Marine Research, Bremerhaven, Germany, [5]Remote Sensing Center, University of Alabama, Tuscaloosa, AL, USA

Key Points:

- We present a novel method for deriving strength and orientation of crystal orientation fabric using double reflections in birefringent ice
- Method reveals a 12-degree rotation of the crystal orientation fabric relative to flow at the center of the North East Greenland Ice Stream
- An asymmetry of the crystal orientation fabric across center of the ice stream indicates more variable flow than previously assumed

Supporting Information:

Supporting Information may be found in the online version of this article.

Correspondence to:

N. F. Nymand,
niels.nymand@nbi.ku.dk

Citation:

Nymand, N. F., Lilien, D. A., Gerber, T. A., Hvidberg, C. S., Steinhage, D., Gogineni, P., et al. (2025). Double reflections in polarized radar data reveal ice fabric in the North East Greenland ice stream. *Geophysical Research Letters*, *52*, e2024GL110453. https://doi.org/10.1029/2024GL110453

Received 30 MAY 2024
Accepted 5 DEC 2024

Abstract The orientation of ice crystals within large ice masses has a strong influence on their mechanical properties, but cannot be directly observed from the surface. The bulk birefringence of anisotropic ice allows us to infer information about the crystal orientation fabric (COF) from polarized radar measurements. Here, we show a new approach for determining the orientation and strength of horizontal COF anisotropy from two radar reflections originating from the same physical layer in birefringent ice. We apply this method to data collected as part of a ground-based radar survey of the North East Greenland Ice Stream. We observe a 12-degree clockwise rotation of the fabric at the center of the ice stream, and a tendency toward a flow-aligned COF further southeast. This asymmetry across the ice-stream centerline adds to growing evidence for a more variable ice stream than previously assumed.

Plain Language Summary The ice in glaciers and ice sheets is composed of crystals, small pieces of ice which can differ in shape and orientation. How ice crystals are arranged is closely linked to how ice sheets move and behave, which is important for predicting changes in polar ice sheets and their impact on sea level rise. Even though the arrangement of the crystals is not directly observable from the surface of ice sheets, we can use specific types of radar measurements to extract general information about how the crystals are arranged. In this study, we present a new approach for doing this. We test the method on data collected as part of a survey of the North East Greenland Ice Stream, which drains 16% of the area of the Greenland Ice Sheet. Our results show that the crystals are not aligned in the way we expected, suggesting that the flow pattern of the ice stream has changed in the past and is not as stable as previously thought.

1. Introduction

The orientation of grains within polycrystalline ice, or crystal orientation fabric (COF), is a fundamental property that governs ice flow. Ice is mechanically anisotropic (Duval et al., 1983), so good estimates of the COF in dynamically interesting areas, such as ice streams, are crucial for constraining the directional viscosity of ice. If ignored, directional hardening or softening caused by the COF can lead to errors when inferring basal conditions (Rathmann & Lilien, 2022), modeling depth-age relationships at ice divides (Martín et al., 2009), or considering the strength of shear margins (Grinsted et al., 2022; Minchew et al., 2018). Improved understanding of the COF can thus contribute to more accurate modeling of ice stream behavior. Since flow variability causes half of the Greenland ice sheet's annual mass loss (Shepherd et al., 2020), this understanding helps reduce uncertainties in future sea level projections.

COF can be measured or inferred in multiple ways. The most direct is using ice cores to derive the orientation of individual grains in the ice (Durand et al., 2006; Montagnat et al., 2014). However, except with highly resolved layering, cores provide only point measurements and absolute orientation is usually lost (Westhoff et al., 2021). Seismics offer an alternative to ice cores by utilizing the elastic anisotropy of ice (Picotti et al., 2015; Smith et al., 2017) to estimate the COF. Another commonly used, and logistically simpler, method for estimating the COF is with polarized radar measurements.

Radar sounding has long been used to recover information about the COF (Hargreaves, 1977). In glacial ice, the dielectric anisotropy of individual ice crystals can alter the polarization state of the transmitted radar waves (Jiracek, 1967). Anisotropic COFs inherit this property, which affects both the travel-time and polarization state

of radar waves. It is common to approximate the COF using a second-order structure tensor, using its eigenvectors and eigenvalues to describe the orientation and strength of the COF. The propagation of radar waves in ice is only sensitive to the second-order structure tensor (Rathmann et al., 2022). In recent years, fully polarimetric radar sounding, including both the co-polarized (transmitting and receiving at the same polarization) and the cross-polarized (transmitting and receiving at orthogonal polarizations) orientations, has become a powerful tool in deriving the horizontal eigenvectors and eigenvalues (Dall, 2020; Ershadi et al., 2022; Fujita et al., 2006; Jordan et al., 2019) using simple radar models together with radar-derived coherence and power anomalies. A new and simpler approach involves measuring the travel-time difference in reflections from the bed or internal layers (Gerber et al., 2023; Zeising et al., 2023) between multiple co-polarized measurements. In anisotropic ice, radar energy must be polarized along the principal axes of the COF, so if the transmitted wave is misaligned with the COF it is split into two waves. These waves have slightly different propagation speeds (Fujita et al., 2006).

Here, we demonstrate that travel-time and amplitude analysis of double reflections in co-polarized data offers a way of inferring the horizontal anisotropy and orientation of the COF, assuming no rotation with depth. First, we present the observations of double reflections, caused by birefringence, collected as part of a larger ground-based radar survey of the North East Greenland Ice Stream (NEGIS), which form the basis of the analysis. Second, we explain why double reflections arise and present a method to use them to infer information about the COF. Third, we derive orientation and horizontal eigenvalue differences of the COF inside NEGIS by applying the new method to the observed double reflections. Lastly, we compare our results to the ice core from the East Greenland Ice Core Project (EastGRIP) (Westhoff et al., 2021; Zeising et al., 2023) and a fabric evolution model presented in Gerber et al. (2023).

2. Data: Ground-Based UWB Polarized Radar

The data used in this study were recorded with a ground-based, ultra-wideband, quad-polarized radar system developed by the University of Alabama (Li et al., 2020). Over the course of two weeks in June and July 2022, we collected more than 500 line-km of radar at NEGIS (Figure 1). The radar operated at center frequency 330 MHz with bandwidth 300 MHz. In this survey, the entire radar system was dragged behind a Skidoo at a speed of about 10 km/hr. The radar electronics and operator were towed inside an enclosed sled (PolyPod, Figure 2). The antenna panels were dragged on an inflatable balloon behind the PolyPod.

The radar switched between four polarization modes (HH, HV, VV, VH), where V and H indicate along-track or across-track polarization of the transmit and receive antennas, at a pulse repetition frequency of 5 kHz. Along with the four polarization modes, we also alternated between two chirp lengths, 10 and 1 μs. We only use the 10 μs data here as it penetrates deeper and, as we will show below, the separation between double reflections depends on the integrated anisotropy of the ice through which the radar waves travel. The antenna is able to distinguish polarizations with a cross-polarization leakage of −30 dB or better for most of the frequency spectrum (Li, 2021).

Processing of the raw radar data was done using custom scripts and consists of coherent integration, pulse compression, incoherent integration, channel integration and interpolation to a consistent grid.

2.1. Double Reflections

In connection with tracking layers, we noticed that layers sometimes split and merge, making the tracking ambiguous. Because we could compare HH and VV, it became apparent that this was most likely an effect of birefringence. This could potentially make the process of automated tracking very difficult, and complicate matching layers between ice core conductivity or dielectric measurements and radar layers.

We interpret these split layers as single physical layers in the ice that reflect two orthogonally polarized waves, split by the birefringence, and returning to the receiver at different times depending on the strength of the birefringence. The partitioning of energy of the two waves, and thereby the recorded amplitudes, is determined by the degree of alignment of the radar antennas and horizontal eigenvectors of the COF. An example of observed double reflections is shown in Figure 2, together with a sketch of the ideas presented here.

Only a very small subset of the data convincingly show these double reflections, most likely due to insufficient misalignment between horizontal eigenvectors of the COF and radar antennas, and most internal reflectors disappear near shear margins where we might expect radar antennas to be misaligned with the COF.

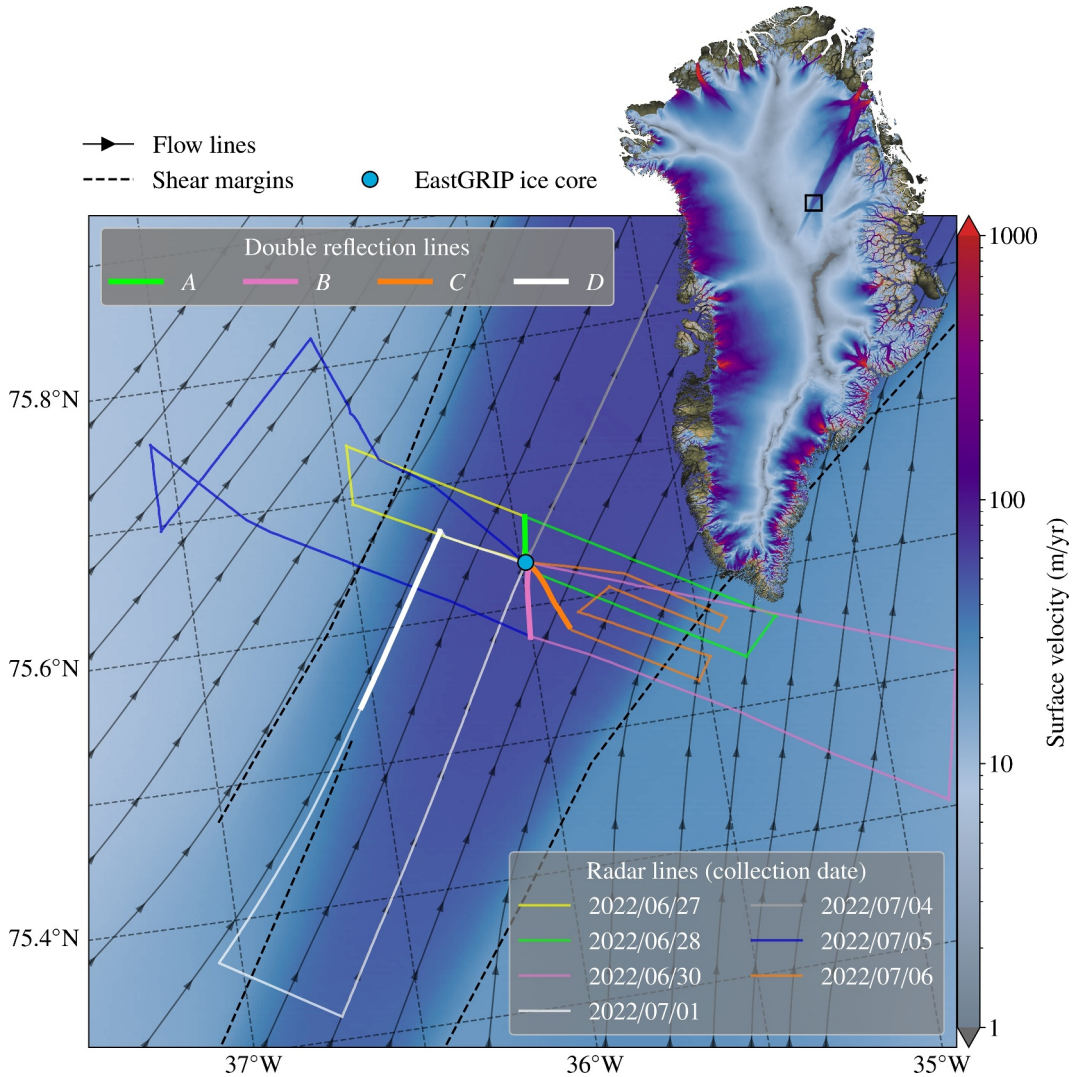

Figure 1. Overview of the 2022 ground-based radar campaign near the EastGRIP drill site, located in the interior, southwestern region of North East Greenland Ice Stream (NEGIS). The black rectangle outlines the survey area. Black dashed lines show the estimated location of the NEGIS shear margins. Black lines with arrowheads show the flow lines. Velocity data was obtained from the NASAs MEaSUREs multi-year data set (Joughin et al., 2016, 2018).

In the following, we provide the theoretical basis for double reflections and demonstrate how it can be used to derive an estimate for the COF.

3. Theory

To explain these double reflections, we need to consider the electromagnetic properties of ice in the VHF to UHF frequency range. In this frequency range, ice crystals are birefringent with permittivity $\varepsilon_{\parallel}$ and $\varepsilon_{\perp}$ parallel and perpendicular to their optical axis, respectively. However, the typical size of individual ice crystals is on the order of 0.5–10 mm (Svensson et al., 2007; Thorsteinsson et al., 1997), which is around two orders of magnitude smaller than the center wavelength of the radar system (~0.5 m in ice). It is therefore appropriate to describe the ice by its bulk properties. For the following we assume that the COF has a vertical eigenvector, pointing along z, and x and y define the two horizontal eigenvectors. The bulk permittivity of ice can be related to the permittivity of a single ice crystal through the bulk permittivity tensor (Fujita et al., 2006),

10.1029/2024GL110453

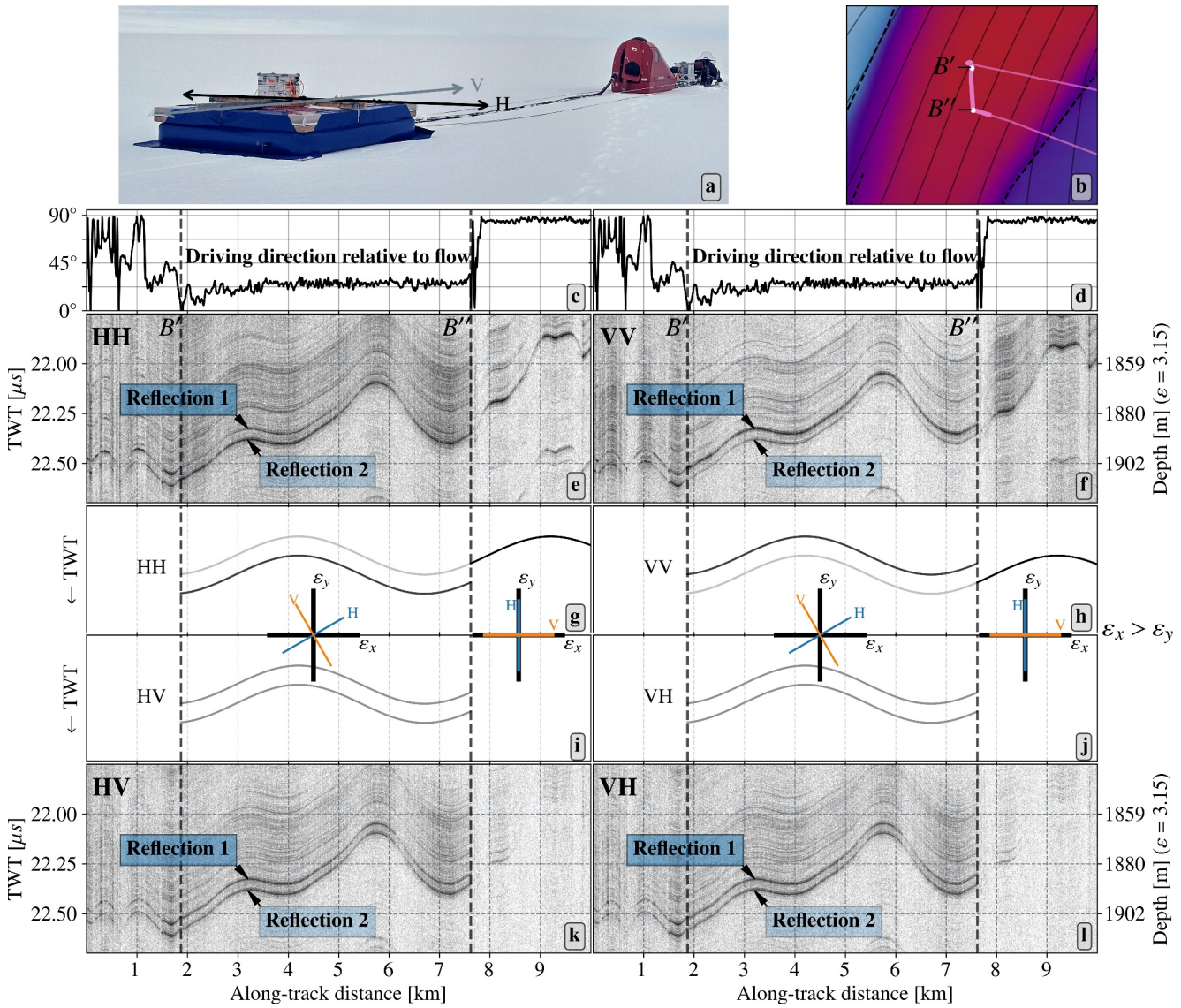

Figure 2. UWB radar and double reflections at North East Greenland Ice Stream. (a) Shows the radar as it was operated in 2022. (c), (d) Show the driving direction of the radar relative to the local flow vector. (e), (f) Is a side by side comparison of HH and VV radargrams collected along the wide pink line on the velocity map in (b), zoomed in on a double reflection $(B' - B'')$. (k, l) Show the HV and VH radargrams. (g)–(j) Show a sketch of double reflections.

$$\boldsymbol{\varepsilon}_b = \begin{pmatrix} \varepsilon_\perp + \Delta\varepsilon\lambda_x & 0 & 0 \\ 0 & \varepsilon_\perp + \Delta\varepsilon\lambda_y & 0 \\ 0 & 0 & \varepsilon_\perp + \Delta\varepsilon\lambda_z \end{pmatrix}, \tag{1}$$

where $\Delta\varepsilon = \varepsilon_\parallel - \varepsilon_\perp$, λ_x, λ_y and λ_z express the normalized eigenvalues of the COF, within the eigenframe of the COF, (x, y, z). We assume the commonly used values $\Delta\varepsilon = 0.034$ and $\varepsilon_\perp = 3.15$ (Fujita et al., 2000).

In the case that $\lambda_x \neq \lambda_y$ and the radar waves propagate vertically, the electrical fields are polarized according to the horizontal principal axes of the permittivity tensor (Fujita et al., 2006), and differently polarized waves will be split. In other words, when the polarization of a radar wave is not aligned with the horizontal eigenvectors, the bulk birefringence of the ice splits the wave into two waves, polarized along x and y. The two waves have different propagation speeds, due to the difference in permittivity. As a result we see two reflections at different travel times from the same layer in the ice.

3.1. Travel Time Difference

If the travel-time difference exceeds the range resolution of the radar we can use it to derive the horizontal eigenvalue difference, $\Delta\lambda = \lambda_x - \lambda_y$, where we define $\lambda_x > \lambda_y$. The two way travel-time (TWT) for polarizations along the two horizontal principal axes, x and y, can be expressed as,

$$t_x(d) = \frac{2d}{c}\sqrt{\varepsilon_\perp + \Delta\varepsilon\lambda_x}, \qquad t_y(d) = \frac{2d}{c}\sqrt{\varepsilon_\perp + \Delta\varepsilon\lambda_y}, \tag{2}$$

where d is the depth measured from the surface of the ice and c is the speed of light in vacuum. These relations can be rearranged to derive $\Delta\lambda$ given the observed travel times,

$$\Delta\lambda = \lambda_x - \lambda_y = \left(\frac{c}{2d}\right)^2 \frac{t_x^2 - t_y^2}{\Delta\varepsilon} = \frac{t_x - t_y}{t_x + t_y}\frac{4\bar{\varepsilon}}{\Delta\varepsilon}, \quad \text{for } d = \frac{c}{\sqrt{\bar{\varepsilon}}}\frac{1}{4}(t_y + t_x), \tag{3}$$

where we define $\lambda_x > \lambda_y$ and $\bar{\varepsilon} = \frac{2}{3}\varepsilon_\perp + \frac{1}{3}\varepsilon_\parallel$ (permittivity of isotropic ice). The error in $\Delta\lambda$ from assuming isotropic travel speeds for estimating d is small compared to the uncertainty from estimating t_x and t_y.

3.2. Relative Amplitude of Double Reflections

The initial relative amplitude of the two downward-propagating waves is determined by ϕ. For the H wave the amplitudes of the two waves, H_x and H_y, can be related to the amplitude of the transmitted wave, H_T, as,

$$H_x = H_T \cos\phi, \quad H_y = H_T \sin\phi. \tag{4}$$

The components of the V wave are computed analogously. As these waves travel through the ice column, each encounters reflectors that reflects a fraction of the wave back toward the surface. If the travel-time difference and amplitudes are large enough, they will appear as two separate reflections to an antenna not aligned with the principal axes. At the surface, the waves will have decreased in amplitude, which we parameterize by two pre-factors, L_x and L_y, which might differ due to anisotropic scattering. The returned amplitudes of the two waves are then L_xH_x and L_yH_y. For a co-polarized measurement, the recorded amplitudes are $L_xH_x \cos\phi$ and $L_yH_y \sin\phi$. The ratio of the amplitudes for the co-polarized measurements can be written as

$$R_{HH} = \frac{L_x}{L_y}\cot^2\phi, \quad R_{VV} = \frac{L_x}{L_y}\tan^2\phi. \tag{5}$$

For an illustration of the relative amplitudes at transmit and receive, see Figure S1 in Supporting Information S1. Amplitudes are usually presented on a logarithmic scale defined by $P_{dB}(a) = 10\log_{10}|a|^2$, where a is the amplitude of the recorded signal and P_{dB} is a measure of the power of the recorded signal expressed in dB. We therefore use a rewritten version of Equation 5,

$$\begin{aligned} \Delta P_{HH} &= 20\log_{10}\left(\frac{L_x}{L_y}\right) - 40\log_{10}(\tan\phi) \\ \Delta P_{VV} &= 20\log_{10}\left(\frac{L_x}{L_y}\right) + 40\log_{10}(\tan\phi), \end{aligned} \tag{6}$$

where ΔP_{HH} and ΔP_{VV} is the power difference in dB between the second and first reflection in HH and VV mode, respectively (Figure 2).

Cross-polarized measurements can be used to eliminate the term depending on L_x and L_y. Following the derivation of Equation 6, the power differences for cross-polarized measurements are,

$$\Delta P_{HV} = \Delta P_{VH} = 20\log_{10}\left(\frac{L_x}{L_y}\right). \tag{7}$$

If cross-polarized measurements were not available, $\Delta P_{HH} - \Delta P_{VV}$ could be used to derive ϕ independent of L_x and L_y. If only one co-polarized measurement were available, cross points might be used to eliminate the first term in Equation 6.

4. Methods

We now apply this theory to the data collected at NEGIS to derive ϕ and $\Delta\lambda$. First, we trace pairs of reflections. The travel-time difference of the reflections allows us to derive the eigenvalue difference using Equation 3. For lines without double reflections the eigenvalue differences is derived by comparing travel-times for layers in HH and VV, similar to cross-point analysis (Gerber et al., 2023).

Determining the fabric orientation from the amplitude of the reflections is more complicated. First, the amplitude is calculated as the maximum value in a 5 sample window centered around the picked reflection. We use the mean and standard deviation of the signal amplitude between the two reflections to define the noise level. Locations where the amplitude of either picked reflector does not exceed the noise level by at least 4 dB are discarded. A schematic of the workflow can be found in the Figure S2 in Supporting Information S1.

We use the cross-polarized data to calculate a corrected power difference,

$$\begin{aligned}\overline{\Delta P}_{HH} &= \Delta P_{HH} - \frac{1}{2}(\Delta P_{HV} + \Delta P_{VH}) = -40\log_{10}(\tan\phi)\\ \overline{\Delta P}_{VV} &= \Delta P_{VV} - \frac{1}{2}(\Delta P_{HV} + \Delta P_{VH}) = 40\log_{10}(\tan\phi).\end{aligned} \tag{8}$$

ϕ can then be estimated independently for HH and VV by rearranging Equation 8 to get

$$\begin{aligned}|\phi_{HH}| &= \arctan\left(10^{-\overline{\Delta P}_{HH}/40}\right)\\ |\phi_{VV}| &= \arctan\left(10^{\overline{\Delta P}_{VV}/40}\right),\end{aligned} \tag{9}$$

where ϕ_{HH} and ϕ_{VV} are independent estimates of ϕ derived from the HH and VV radargrams, respectively.

Equation 9 has two solutions; the sign of ϕ is ambiguous without additional information. Minor fluctuations in the driving direction, and consequently in radar orientation during data collection, allow the sign to be determined. If we assume that the orientation of the COF changes over much greater distances than the radar orientation, we can determine the sign of ϕ by cross-correlating the along-track gradient of the power difference with the along-track gradient of $|\phi|$. For the HH case,

$$\begin{aligned}\phi > 0, \text{ if } \quad \operatorname{sign}\left(\frac{d(\Delta P_{HH})}{ds}\right) &= -\operatorname{sign}\left(\frac{\partial|\phi_{HH}|}{\partial s}\right)\\ \phi < 0, \text{ if } \quad \operatorname{sign}\left(\frac{d(\Delta P_{HH})}{ds}\right) &= +\operatorname{sign}\left(\frac{\partial|\phi_{HH}|}{\partial s}\right)\end{aligned} \tag{10}$$

where s represents the along-track coordinate. For VV we just flip the signs of Equation 10. To determine the COF orientation, we thus calculate two estimates of ϕ, each following Equation 9 to get $|\phi|$ and Equation 10 to find $\operatorname{sign}(\phi)$.

Because the energy is split between two waves, we need strong reflectors for the signal to rise above the noise. Across different radar lines, we found three reflectors that were consistently well suited to carry out the analysis. They are approximately 2 km deep at EastGRIP and have been found all over Greenland (Dahl-Jensen et al., 2003; Gerber et al., 2021; Jacobel & Hodge, 1995; NEEM Community Members, 2013). Because they are strong reflectors and lie in an otherwise relatively echo-free zone, they are easily picked and rise well above the noise. They are also deep enough for the travel-time difference to be significant at the COF strength around NEGIS. We thus obtain up to six independent estimates of the fabric strength and orientation (two polarizations times three layers) at every radar trace.

This method relies on these reflections originating from one physical layer, not two closely spaced, orthogonally scattering layers that mimic the relative amplitudes of double reflections. Having multiple layers showing the same pattern can help distinguish between these possibilities. The HV or VH data can also reveal if the layers are subject to strong anisotropic scattering.

5. Results

Across the center of the ice stream, we observe a small increase in the rotation of the COF with respect to flow as we move from B'' toward the center at B' and a constant rotation of 12 ± 5° from the center at A'' to A'. This is followed by a generally increasing eigenvalue difference from $\Delta\lambda = 0.42$ at B'' to $\Delta\lambda = 0.7$ at A'. Unlike most glacier settings, this implies that c-axes are primarily horizontal, associated with flow convergence and lateral compression. Upstream with increasing proximity to the southeastern shear margin (C'' to C'), we find a more flow-aligned COF that tends to counterclockwise rotation of the COF at C'. The signal-to-noise ratio generally decreases from C' to C'', decreasing confidence in the orientation estimates toward C''. Our uncertainty estimates do not fully capture this variation (see Text S1 and Figure S8 in Supporting Information S1 for details). At the northwestern shear margin (D' to D''), we find a constant clockwise rotation of the COF of about 40° with a small increase in the eigenvalue difference from $\Delta\lambda = 0.65$ to $\Delta\lambda = 0.75$ toward D''. Figure 3b includes flow parallel and perpendicular lines with no observed double reflections. Eigenvalue differences for these lines were derived by comparing travel times between the HH- and VV-radargrams for the same three layers used to analyze double reflections. Comparison of HH and VV travel time indicates nearly constant eigenvalue difference along the ice-stream center. The across flow line is asymmetric about the ice-stream center, with a general increase from the southeast to the northwest. Results derived for radar lines 2022/06/27 and 2022/07/05 in Figure 1, are omitted due to overlap with 2022/06/28 and 2022/06/30, respectively. The overlapping lines agree within their respective uncertainties, and detailed results can be found in Figures S4–S8 in Supporting Information S1.

6. Discussion

Our results suggest that the eigenframe of the COF is rotated about 12° relative to flow close to the center of the ice stream. This seemingly contrasts with the reconstruction based on visual stratigraphy of the EastGRIP ice core (Westhoff et al., 2021), which finds that the COF is generally aligned with flow. However, a 12-degree rotation is small compared to the spread of reconstructed c-axis azimuths (Westhoff et al., 2021, Figure 10c_3). The COF above 1,375 m, where the ice core orientation has been reconstructed, may be rotated relative to the COF below, though the radar only records a cumulative effect. Only the top 1,714 m of the ice-core eigenvalues have been published (Weikusat et al., 2022; Zeising et al., 2023), and assuming a constant COF below 1,714 m and isotropic at the surface, the depth-averaged horizontal eigenvalue difference from the ice core is $\Delta\lambda = 0.53 \pm 0.01$ at the depth of the three radar layers. This is in near-perfect agreement with our closest estimate to EastGRIP (A'') which gives $\Delta\lambda = 0.52 \pm 0.01$, which is also in good agreement with the results derived from ApRES (Zeising et al., 2023).

6.1. Method Limitations

Our new method leverages characteristics of the study site and radar to overcome limitations that may prove problematic when attempting to apply the method in other settings. The method assumes that the orientation of the eigenvectors remains constant throughout the illuminated ice column. This is partly supported by the ice-core reconstruction, which does not suggest a changing eigenframe in the interval 1,375 m–2120 m (Westhoff et al., 2021). The method works best at relatively large misalignment with the eigenvectors, approximately 45° ± 15°, to produce sufficient amplitude differences to estimate orientation. A radar with cross-pol leakage comparable to the amplitude difference (∼5–10 dB) may not observe power differences between the two layers, and thus might be confined to estimating $\Delta\lambda$ but not orientation. Radars with low range resolution or low transmit power might struggle to produce strong double reflections at a depth where the travel-time difference exceeds the range resolution. The eigenvalue difference resolvable for a given bandwidth, B, can be expressed as,

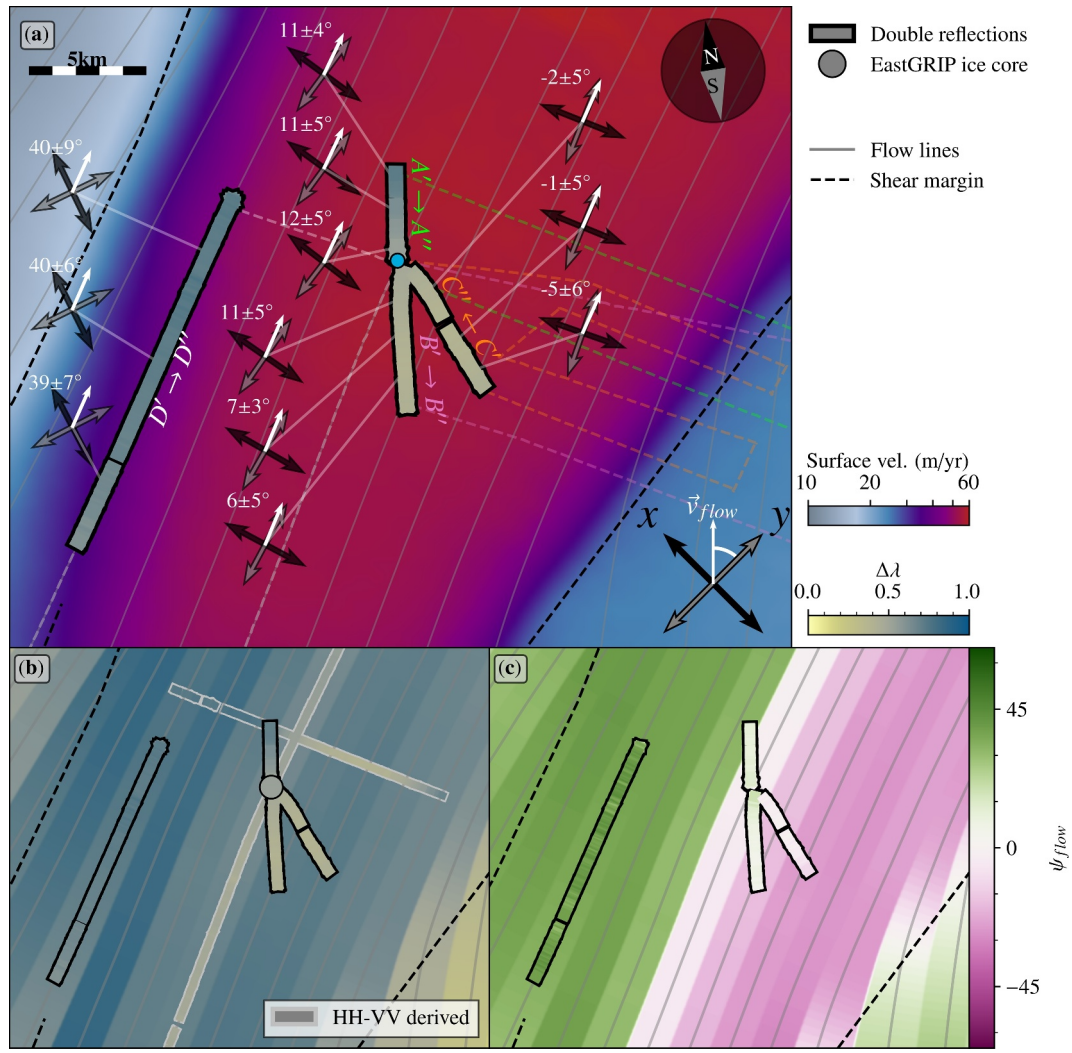

Figure 3. Orientation and strength of COF, derived from double reflections, plotted on top of panel (a) surface velocity map of North East Greenland Ice Stream (Joughin et al., 2016) and (b)–(c) modeled fabric from (Gerber et al., 2023). (a) The black and gray arrows show the horizontal principal components of the COF, x and y respectively, as derived from the amplitude differences. Arrows show mean values with depth (i.e., across three layers) and distance for sections of each radar line (thirds). The white arrows are the local flow directions, and the white number is the angle between the flow vector and the smallest eigenvalue. Explanation of orientation uncertainty can be found in Text S1 in Supporting Information S1. Gray solid lines show flow lines. The yellow-blue colors of the wide lines show the depth-averaged horizontal eigenvalue difference derived from the travel-time difference of the double reflections. (b) Shows eigenvalue differences from double reflections, as well as flow parallel and perpendicular lines with no observed double reflections, plotted on top of the depth averaged modeled horizontal eigenvalue difference. (c) Shows the orientation derived from the double reflections plotted on top of the modeled orientations, where ψ_{flow} is the angle between flow and y. Primed and double primed letters with arrow show the traveling direction from the start to the end of the double reflection lines, respectively.

$$\Delta\lambda_{\min} = \frac{c}{z\,B}\frac{\sqrt{\bar{\varepsilon}}}{\Delta\varepsilon} \approx \begin{cases} 0.26 & \text{for}: \ B = 30MHz, \quad z = 2km \\ 0.09 & \text{for}: \ B = 85MHz, \quad z = 2km \\ 0.04 & \text{for}: \ B = 200MHz, \quad z = 2km \\ 0.026 & \text{for}: \ B = 300MHz, \quad z = 2km \end{cases} \tag{11}$$

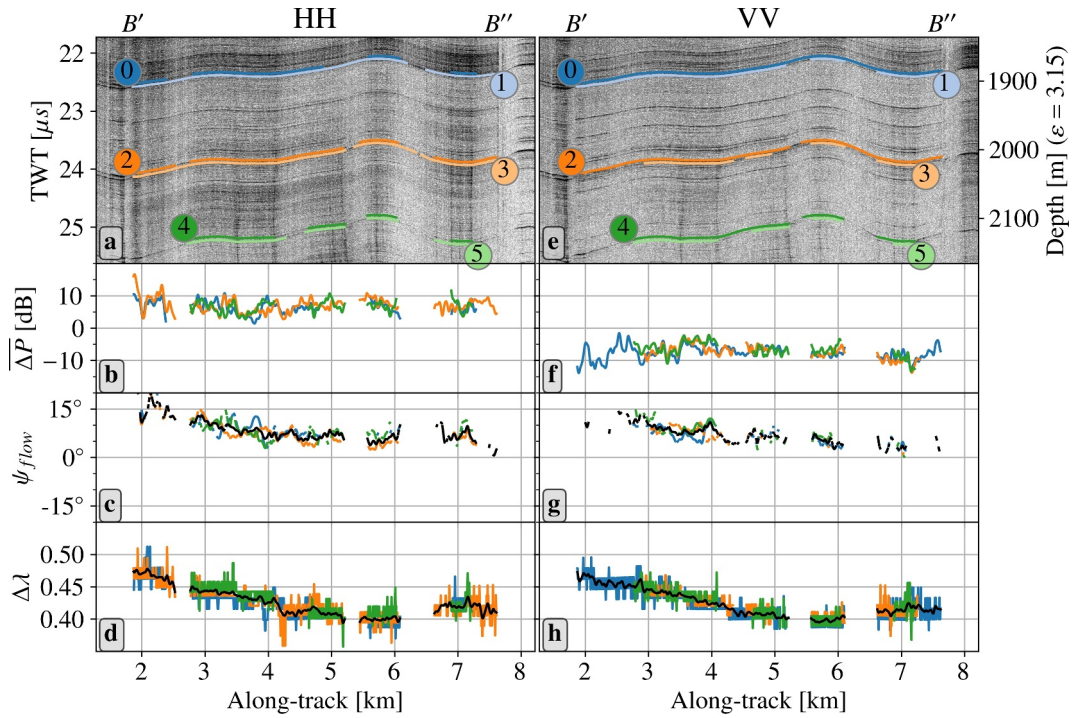

Figure 4. Detailed overview of results from line *B* in Figure 3. (a) HH-radargram where visible double reflections have been picked in pairs (0, 1), (2, 3), and (4, 5), with the corrected amplitude differences plotted below in panel (b) for each layer, blue, orange and green. (c) Calculated orientations of the smallest eigenvalue relative to flow for each layer with a smoothed mean plotted on top in black. (d) Horizontal eigenvalue difference based on the travel-time difference of the reflection pairs picked in panel (a). (e)–(h) as in panels (a)–(d), but for VV.

where the range resolution of a radar system with bandwidth B is $\frac{c}{2B\sqrt{\varepsilon}}$ (Skolnik, 2001). Figure S3 in Supporting Information S1 shows a radargram from the MCoRDS radar (Paden et al., 2014), which has been flown for thousands of kilometers over Greenland and Antarctica, with probable double reflections. For radar data with double reflections, every sample is a superposition of scattering events of the two wave components, making interpretation difficult except for bright isolated layers. The layers that we have used (see Figure 4) are found all over Greenland, and are located in an otherwise relatively echo free zone (Dahl-Jensen et al., 2003; Gerber et al., 2021; Jacobel & Hodge, 1995; NEEM Community Members, 2013), suggesting that the method might work in other sections of the ice sheet with strong horizontal anisotropy. We encourage future studies using ice penetrating radar data to consider how double reflections may influence their interpretations.

6.2. Comparison With a Fabric Development Model

Comparison between our results and the horizontal anisotropy predicted by a fabric development model offers potential insight into the glaciological conditions at NEGIS (Figures 3b and 3c). We compare our results to a model that simulated COF development under the assumptions that flow has been steady for the past ~10k years and COF develops solely by lattice rotation. In contrast to the observations, which show symmetry of the orientation and horizontal eigenvalue difference across a plane parallel to but southeast of the current ice-stream centerline, the model predicts symmetry across the ice-stream centerline. That two independently observed parameters, the horizontal eigenvalue difference and orientation, disagree with the model results for the southeastern part of the ice stream suggests that model assumptions do not hold. While there is some uncertainty in the robustness of the modeled eigenvalue difference due to recrystallization (Richards et al., 2023), the lack of rotation of the COF relative to flow is tied to the fundamental physics of COF development and the assumption of steady flow. Since the modern centerline does not cross a shear margin, the ice does not experience shear or rotation, so current understanding of COF development under lattice rotation or recrystallization suggests that if flow has been steady there should be symmetry about the ice-stream centerline. We thus suggest that the assumption of steady-state flow is mainly responsible for the disagreement between model and observations.

The widening of the shear margins observed in Grinsted et al. (2022) suggests a variable ice stream rather than one in steady state. Franke et al. (2022) observed relic ice streams north of present day NEGIS that were likely active during the Holocene. Jansen et al. (2024) found that the current shear margins of NEGIS were fully formed only 2000 years ago. These three independent lines of evidence all support recent flow changes in or around NEGIS. Conversely, the model results from Gerber et al. (2023) assumed steady flow in the past, so mismatch between model and data could suggest that the COF has not yet adjusted to the new flow configuration. For example, a recent northward migration of the ice stream could explain why the COF is rotated relative to modern flow. Thus, the mismatch between our results and the model could be evidence of an ice stream with a more variable past than commonly assumed.

7. Conclusion

Using double reflections recorded at NEGIS with a new, high-resolution radar system, we have derived information about the COF, namely the orientation of the horizontal eigenframe and the horizontal eigenvalue difference. This new method may enable simpler radar systems with a single, linearly polarized antenna to estimate COF along a radar line, subject to the conditions that $\Delta\lambda$ is large enough and the radar has sufficient power and sensitivity to sound layers deep enough that travel-time differences exceed the range resolution of the radar. We find a strong asymmetry in both the orientation and eigenvalue differences across the modern center of NEGIS. This contrasts with a fabric development model (Gerber et al., 2023), which shows approximate symmetry across the center of the ice stream under the assumption that ice flow has remained steady for the last ∼10 kyr; the model/data mismatch likely stems from that assumption. Together with recent studies about the age and present-day widening of the NEGIS shear margins (Grinsted et al., 2022; Jansen et al., 2024), as well as the discovery of relic ice streams in northern Greenland (Franke et al., 2022), this work is another piece of evidence for a more variable NEGIS than previously assumed.

Data Availability Statement

Radar data, horizontal eigenvalue differences, COF orientations and code are available at Nymand and Dahl-Jensen (2024). Greenland surface velocity data are available at Joughin et al. (2016). ImpDAR Software used for picking layers in radargrams are available at Lilien et al. (2020). EastGRIP ice core eigenvalues down to 1714 m are available at Weikusat et al. (2022).

Acknowledgments
This research has been supported by the Villum Fond (Grant 16572), the EGRIP camp and logistical team, the Canada Excellence Research Chairs Program, the Novo Nordisk Foundation (Grant NNF23OC0081251), and the Danmarks Frie Forskningsfond (Grant 2032-00364B). EGRIP is directed and organized by the Centre for Ice and Climate at the Niels Bohr Institute, University of Copenhagen. It is supported by funding agencies and institutions in Denmark (A. P. Møller Foundation, University of Copenhagen), USA (US National Science Foundation, Office of Polar Programs), Germany (Alfred Wegener Institute, Helmholtz Centre for Polar and Marine Research), Japan (National Institute of Polar Research and Arctic Challenge for Sustainability), Norway (University of Bergen and Trond Mohn Foundation), Switzerland (Swiss National Science Foundation), France (French Polar Institute Paul-Emile Victor, Institute for Geosciences and Environmental research), Canada (University of Manitoba) and China (Chinese Academy of Sciences and Beijing Normal University). We thank the two anonymous reviewers and Nicholas Holschuh for their insightful feedback and edits, which have helped improve the manuscript. We also thank editor Mathieu Morlighem for overseeing the review process and providing helpful input to improve the manuscript.

References

Dahl-Jensen, D., Gundestrup, N., Gogineni, S. P., & Miller, H. (2003). Basal melt at North grip modeled from borehole, ice-core and radio-echo sounder observations. *Annals of Glaciology*, *37*, 207–212. https://doi.org/10.3189/172756403781815492

Dall, J. (2020). Estimation of crystal orientation fabric from airborne polarimetric ice sounding radar data. In *IGARSS 2020 - 2020 IEEE international geoscience and remote sensing symposium* (pp. 2975–2978). https://doi.org/10.1109/IGARSS39084.2020.9323437

Durand, G., Gagliardini, O., Thorsteinsson, T., Svensson, A., Kipfstuhl, S., & Dahl-Jensen, D. (2006). Ice microstructure and fabric: An up-to-date approach for measuring textures. *Journal of Glaciology*, *52*(179), 619–630. https://doi.org/10.3189/172756506781828377

Duval, P., Ashby, M. F., & Anderman, I. (1983). Rate-controlling processes in the creep of polycrystalline ice. *The Journal of Physical Chemistry*, *87*(21), 4066–4074. https://doi.org/10.1021/j100244a014

Ershadi, M. R., Drews, R., Martín, C., Eisen, O., Ritz, C., Corr, H., et al. (2022). Polarimetric radar reveals the spatial distribution of ice fabric at domes and divides in East Antarctica. *The Cryosphere*, *16*(5), 1719–1739. https://doi.org/10.5194/tc-16-1719-2022

Franke, S., Bons, P., Westhoff, J., Weikusat, I., Binder, T., Streng, K., et al. (2022). Holocene ice-stream shutdown and drainage basin reconfiguration in northeast Greenland. *Nature Geoscience*, *15*(12), 1–7. https://doi.org/10.1038/s41561-022-01082-2

Fujita, S., Maeno, H., & Matsuoka, K. (2006). Radio-wave depolarization and scattering within ice sheets: A matrix-based model to link radar and ice-core measurements and its application. *Journal of Glaciology*, *52*(178), 407–424. https://doi.org/10.3189/172756506781828548

Fujita, S., Matsuoka, T., Ishida, T., Matsuoka, K., & Mae, S. (2000). A summary of the complex dielectric permittivity of ice in the megahertz range and its applications for radar sounding of polar ice sheets. In *Physics of ice core records* (pp. 185–212).

Gerber, T., Lilien, D., Rathmann, N., Franke, S., Young, T. J., Valero-Delgado, F., et al. (2023). Crystal orientation fabric anisotropy causes directional hardening of the northeast Greenland ice stream. *Nature Communications*, *14*(1), 2653. https://doi.org/10.1038/s41467-023-38139-8

Gerber, T. A., Hvidberg, C. S., Rasmussen, S. O., Franke, S., Sinnl, G., Grinsted, A., et al. (2021). Upstream flow effects revealed in the east grip ice core using Monte Carlo inversion of a two-dimensional ice-flow model. *The Cryosphere*, *15*(8), 3655–3679. https://doi.org/10.5194/tc-15-3655-2021

Grinsted, A., Hvidberg, C., Lilien, D., Rathmann, N., Karlsson, N., Gerber, T., et al. (2022). Accelerating ice flow at the onset of the northeast Greenland ice stream. *Nature Communications*, *13*(1), 5589. https://doi.org/10.1038/s41467-022-32999-2

Hargreaves, N. D. (1977). The polarization of radio signals in the radio echo sounding of ice sheets. *Journal of Physics D: Applied Physics*, *10*(9), 1285–1304. https://doi.org/10.1088/0022-3727/10/9/012

Jacobel, R. W., & Hodge, S. M. (1995). Radar internal layers from the Greenland summit. *Geophysical Research Letters*, *22*(5), 587–590. https://doi.org/10.1029/95GL00110

Jansen, D., Franke, S., Bauer, C., Binder, T., Dahl-Jensen, D., Eichler, J., et al. (2024). Shear margins in upper half of northeast Greenland ice stream were established two millennia ago. *Nature Communications*, *15*(1), 1193. https://doi.org/10.1038/s41467-024-45021-8

Jiracek, G. R. (1967). *Radio sounding of antarctic ice (Tech. Rep.)*. Geophysical & Polar Research Center, University of Wisconsin.

Jordan, T. M., Schroeder, D. M., Castelletti, D., Li, J., & Dall, J. (2019). A polarimetric coherence method to determine ice crystal orientation fabric from radar sounding: Application to the neem ice core region. *IEEE Transactions on Geoscience and Remote Sensing*, *57*(11), 8641–8657. https://doi.org/10.1109/TGRS.2019.2921980

Joughin, I., Smith, B., Howat, I., & Scambos, T. (2016). Measures multi-year Greenland ice sheet velocity mosaic, version 1 [Dataset]. https://doi.org/10.5067/QUA5Q9SVMSJG

Joughin, I., Smith, B. E., & Howat, I. M. (2018). A complete map of Greenland ice velocity derived from satellite data collected over 20 years. *Journal of Glaciology*, *64*(243), 1–11. https://doi.org/10.1017/jog.2017.73

Li, L. (2021). *Ultrawide-band polarimetric multi-channel radar for measurements of polar ice sheets (Ph.D. Thesis)*. The University of Alabama, Electrical Engineering.

Li, L., Yan, J.-B., Gogineni, S., O'Neill, C., Dahl-Jensen, D., Simpson, C. D., et al. (2020). Ground-based ultra wideband dual-polarized radar sounding of Greenland ice sheets. In *IGARSS 2020 - 2020 IEEE international geoscience and remote sensing symposium* (pp. 1417–1419). https://doi.org/10.1109/IGARSS39084.2020.9323479

Lilien, D., Hills, B., Driscol, J., Jacobel, R., & Christianson, K. (2020). ImpDAR: An open-source impulse radar processor. *Annals of Glaciology*, *61*(81), 1–10. https://doi.org/10.1017/aog.2020.44

Martín, C., Gudmundsson, G. H., Pritchard, H. D., & Gagliardini, O. (2009). On the effects of anisotropic rheology on ice flow, internal structure, and the age-depth relationship at ice divides. *Journal of Geophysical Research*, *114*(F4), F04001. https://doi.org/10.1029/2008JF001204

Minchew, B. M., Meyer, C. R., Robel, A. A., Gudmundsson, G. H., & Simons, M. (2018). Processes controlling the downstream evolution of ice rheology in glacier shear margins: Case study on rutford ice stream, west Antarctica. *Journal of Glaciology*, *64*(246), 583–594. https://doi.org/10.1017/jog.2018.47

Montagnat, M., Azuma, N., Dahl-Jensen, D., Eichler, J., Fujita, S., Gillet-Chaulet, F., et al. (2014). Fabric along the neem ice core, Greenland, and its comparison with grip and NGRIP ice cores. *The Cryosphere*, *8*(4), 1129–1138. https://doi.org/10.5194/tc-8-1129-2014

NEEM Community Members. (2013). Eemian interglacial reconstructed from a Greenland folded ice core. *Nature*, *493*(7433), 489–494. https://doi.org/10.1038/nature11789

Nymand, N. F., & Dahl-Jensen, D. (2024). Doble reflection data at the North East Greenland ice stream [Dataset]. University of Copenhagen. https://doi.org/10.17894/UCPH.89B622D6-F62F-43D5-B754-7A40748120B1

Paden, J., Li, J., Leuschen, C., Rodriguez-Morales, F., & Hale, R. (2014). Ice bridge mcords l1b geo located radar echo strength profiles, version 2. *NASA National Snow and Ice Data Center Distributed Active Archive Center*. https://doi.org/10.5067/90S1XZRBAX5N

Picotti, S., Vuan, A., Carcione, J. M., Horgan, H. J., & Anandakrishnan, S. (2015). Anisotropy and crystalline fabric of Whillans ice stream (west Antarctica) inferred from multicomponent seismic data. *Journal of Geophysical Research: Solid Earth*, *120*(6), 4237–4262. https://doi.org/10.1002/2014JB011591

Rathmann, N. M., & Lilien, D. A. (2022). Inferred basal friction and mass flux affected by crystal-orientation fabrics. *Journal of Glaciology*, *68*(268), 236–252. https://doi.org/10.1017/jog.2021.88

Rathmann, N. M., Lilien, D. A., Grinsted, A., Gerber, T. A., Young, T. J., & Dahl-Jensen, D. (2022). On the limitations of using polarimetric radar sounding to infer the crystal orientation fabric of ice masses. *Geophysical Research Letters*, *49*(1), e2021GL096244. https://doi.org/10.1029/2021GL096244

Richards, D. H., Pegler, S. S., Piazolo, S., Stoll, N., & Weikusat, I. (2023). Bridging the gap between experimental and natural fabrics: Modeling ice stream fabric evolution and its comparison with ice-core data. *Journal of Geophysical Research: Solid Earth*, *128*(11), e2023JB027245. https://doi.org/10.1029/2023JB027245

Shepherd, A., Ivins, E., Rignot, E., Smith, B., van den Broeke, M., Velicogna, I., & Team, I. (2020). Mass balance of the Greenland ice sheet from 1992 to 2018. *Nature*, *579*(7798), 233–239. https://doi.org/10.1038/s41586-019-1855-2

Skolnik, M. (2001). *Introduction to radar systems* (3rd ed.). McGraw-Hill.

Smith, E. C., Baird, A. F., Kendall, J. M., Martín, C., White, R. S., Brisbourne, A. M., & Smith, A. M. (2017). Ice fabric in an Antarctic ice stream interpreted from seismic anisotropy. *Geophysical Research Letters*, *44*(8), 3710–3718. https://doi.org/10.1002/2016GL072093

Svensson, A., Durand, G., Mathiesen, J., Persson, A., & Dahl-Jensen, D. (2007). Texture of the upper 1000 m in the grip and north grip ice cores. (Vol. *68*).

Thorsteinsson, T., Kipfstuhl, J., & Miller, H. (1997). Textures and fabrics in the grip ice core. *Journal of Geophysical Research*, *102*(C12), 26583–26599. https://doi.org/10.1029/97JC00161

Weikusat, I., Stoll, N., Kerch, J., Eichler, J., Jansen, D., & Kipfstuhl, S. (2022). Crystal c-axes (fabric analyser G50) of ice core samples (vertical thin sections) collected from the polar ice core EGRIP, 111-1714 m depth [Dataset]. *PANGAEA*. https://doi.org/10.1594/PANGAEA.949248

Westhoff, J., Stoll, N., Franke, S., Weikusat, I., Bons, P., Kerch, J., et al. (2021). A stratigraphy-based method for reconstructing ice core orientation. *Annals of Glaciology*, *62*(85–86), 191–202. https://doi.org/10.1017/aog.2020.76

Zeising, O., Gerber, T., Eisen, O., Ershadi, M., Stoll, N., Weikusat, I., & Humbert, A. (2023). Improved estimation of the bulk ice crystal fabric asymmetry from polarimetric phase co-registration. *The Cryosphere*, *17*(3), 1097–1105. https://doi.org/10.5194/tc-17-1097-2023